

Extreme r-process enhanced stars at high metallicity in Fornax*

M. REICHERT,¹ C. J. HANSEN,^{2,3} AND A. ARCONES^{1,4}

¹*Technische Universität Darmstadt, Institut für Kernphysik, Schlossgartenstr. 2, 64289 Darmstadt, Germany*

²*Max-Planck-Institut für Astronomie, Königstuhl 17, D-69117 Heidelberg, Germany*

³*Copenhagen University, Dark Cosmology Centre, The Niels Bohr Institute, Vibenshuset, Lyngbyvej 2, DK-2100 Copenhagen, Denmark*

⁴*GSI Helmholtzzentrum für Schwerionenforschung GmbH, Planckstr. 1, D-64291 Darmstadt, Germany*

(Received -; Revised -; Accepted -)

Submitted to APJ

ABSTRACT

We present and discuss three extremely r-process enhanced stars located in the massive dwarf spheroidal galaxy Fornax. These stars are very unique with an extreme Eu enrichment ($1.25 \leq [\text{Eu}/\text{Fe}] \leq 1.45$) at high metallicities ($-1.3 \leq [\text{Fe}/\text{H}] \leq -0.8$). They have the largest Eu abundances ever observed in a dwarf galaxy opening new opportunities to further understand the origin of heavy elements formed by the r-process. We derive stellar abundances of Co, Zr, La, Ce, Pr, Nd, Er, and Lu using 1-dimensional, local thermodynamic equilibrium (LTE) codes and model atmospheres in conjunction with state-of-the-art yield predictions. We derive Zr in the largest sample of stars (105) known to date in a dwarf galaxy. Accurate stellar abundances combined with a careful assessment of the yield predictions have revealed three metal-rich stars in Fornax showing a pure r-process pattern. We define a new class of stars, namely Eu-stars, as r-II stars (i.e., $[\text{Eu}/\text{Fe}] > 1$) at high metallicities (i.e., $[\text{Fe}/\text{H}] \gtrsim -1.5$). The stellar abundance pattern contains Lu, observed for the first time in a dwarf galaxy, and reveals that a late burst of star formation has facilitated extreme r-process enhancement late in the galaxy's history (< 4 Gyr ago). Due to the large uncertainties associated with the nuclear physics input in the yield predictions, we cannot yet determine the r-process site leading to the three Eu-stars in Fornax. Our results demonstrate that extremely r-rich stars are not only associated with ultra faint low-mass dwarf galaxies, but can be born also in massive dwarf galaxies.

Keywords: stars: chemically peculiar — galaxies: dwarf — galaxies: individual — nuclear reactions, nucleosynthesis, abundances

1. INTRODUCTION

The creation of heavy elements poses a number of open and interesting questions going from a small scales to the largest scales including formation of stars or even galaxies. Recent studies of Milky Way (MW) halo stars have shown that stars rich in neutron-capture elements may have originated in now dissolved (ultra faint) dwarf galaxies (Roederer et al. 2018a). Limited to smaller sample sizes, the results seem to indicate that stars with

the strongest rapid neutron-capture process (r-process) enhancement have formed ex situ and later been accreted into the MW. This makes dwarf galaxies excellent study cases for understanding the r-process.

Fornax (Fnx) is one of the most massive dwarf spheroidal (dSph) in the Local Group (LG). It shows a unique star formation history with a sudden increase of star formation only ~ 4 Gyr ago (de Boer et al. 2012; Lemasle et al. 2014; Hendricks et al. 2014; Weisz et al. 2014; Rusakov et al. 2021). Furthermore, Fornax might currently have gas left, however, this is still under debate (Bouchard et al. 2006). All dwarf galaxies show individual trades and chemical imprints (Grebel 1997; Tolstoy et al. 2009).

Corresponding author: M. Reichert
mreichert@theorie.ikp.physik.tu-darmstadt.de

* Based on data obtained from the ESO reduced archive. Program IDs: 080.B-0784(A), 171.B-0588(A), 71.B-0641(A).

Here we present three Fornax stars with extreme high Eu abundances (rII stars, $[\text{Eu}/\text{Fe}]^1 > 1$, Beers & Christlieb 2005) at high metallicities. Moreover, we report a large study of the neutron-capture element Zr in the dSph Fornax. Our study presents the first detection of the heavy element Lu in a dSph. In contrast to most r-process enriched stars, typically found at low-metallicities ($[\text{Fe}/\text{H}] \sim -2$), the three Eu-stars in Fornax are relatively metal-rich ($[\text{Fe}/\text{H}] \sim -1$). Hence, we use them to understand the astrophysical source of the r-process by comparing to various yield predictions.

Stars with peculiar enhanced r-process abundances have rarely been observed at these high metallicities. Most of them are clearly members of a dSph galaxy, e.g., Ursa Minor (Cos 82, Shetrone et al. 2001; Aoki et al. 2007; Sadakane et al. 2004 or Sculptor, SCMS 982, Geisler et al. 2005; Skúladóttir et al. 2020). We note that there are also neutron-capture enhanced stars at similar metallicities reported already by Letarte et al. (2010) in Fornax, which were not found in Letarte et al. (2018) and Reichert et al. (2020). Also MW field stars, for example, 2MASS 18174532-3353235 (Johnson et al. 2013) a possible bulge contender, shows a high neutron-capture enhancement at a high metallicity. Moreover, some halo stars show similar abundance enhancements and are thought to be accreted into the MW halo, as indicated by a low $[\alpha/\text{Fe}]$ ratio (J1124+4535, Xing et al. 2019), while for others, their origin is, however, not so clear. Also HD 222925 is r-rich and located in the halo, but due to its highly eccentric and retrograde orbit it has been suggested to be accreted from a satellite galaxy (Roederer et al. 2018a). By looking at the alpha-abundances and fitting a knee to the stellar population, the dSph mass can be assessed. Following the fit of the α -knee of Reichert et al. (2020, Eq. 6), the host environment of this star must have at least the size of Sagittarius or Fornax and an accretion scenario may therefore be possible (see also Roederer et al. 2018b, for a discussion on the origin of HD 222925).

The astrophysical sites of the r-process are still under discussion, even if recent kilonova (Abbott et al. 2017; Watson et al. 2019) has shown that neutron star mergers (NSM) can produce heavy elements. Galactic chemical evolution (GCE) models (e.g., Matteucci et al. 2014; Côté et al. 2019; Kobayashi et al. 2020) suggest that an additional site may be active in our galaxy. An exciting possibility are magneto-rotational supernovae (MR-SNe; Winteler et al. 2012; Nishimura et al. 2015, 2017; Mösta

Table 1. Different FLAMES/GIRAFFE setups showing minimum and maximum wavelength coverage and resolving power (R).

Grating	$\lambda_{min}[\text{Å}]$	$\lambda_{max}[\text{Å}]$	R
HR10	5339	5619	19800
HR13	6120	6405	22500
HR14	6308	6701	17740
LR8	8206	9400	6500

et al. 2018; Reichert et al. 2021). Stars at intermediate metallicities are highly mixed and remain poorly studied in the GCE scheme. Also collapsars (Siegel et al. 2019; Miller et al. 2020; Just et al. 2021) have been discussed as a potential site. Our results indicate that both sites, NSM and MR-SNe, can explain the Eu-stars and probe a late star formation burst in Fornax.

This paper is organised as follows. In Sect. 2, we present the observations, sample, and stellar parameters. The abundances are shown in Sect. 3 including the largest Zr sample in a dwarf galaxy and heavy neutron-capture elements with focus on Eu and the first Lu detection in a dwarf galaxy. In Sect. 4, we discuss in detail the possible origin of the Eu-stars, which is associated with one r-process event and requires late star formation. Finally, we conclude in Sect. 5.

2. OBSERVATIONS, SAMPLE, AND STELLAR PARAMETERS

2.1. Observations

We present four Fornax stars including three with anomalous high Eu ($1.25 \leq [\text{Eu}/\text{Fe}] \leq 1.45$). The quality of the available observations allows for an accurate and precise determination of abundances (typically to within ± 0.2 dex). The stars were observed at high and low resolution with FLAMES/GIRAFFE (Pasquini et al. 2002) with the setups HR10, HR13, HR14, and LR8 (see Table 1). The LR8 setup (Battaglia et al. 2006) is used here only for radial velocity determinations. We use reduced spectra from the ESO archive² and perform the data processing (sky correction, radial velocity shifts, co-adding, and normalisation of the spectra) as in Reichert et al. (2020).

2.2. Sample

Our sample consists of Fornax stars from Reichert et al. 2020 who analysed 380 stars in dSph galaxies. The stars have been extracted from the reduced ESO

¹ $[\text{Eu}/\text{Fe}] = \log(N_{\text{Eu}}/N_{\text{Fe}}) - \log(N_{\text{Eu}}/N_{\text{Fe}})_{\odot}$, with the number of europium and iron atoms per cm^3 , N_{Eu} and N_{Fe} .

² https://archive.eso.org/wdb/wdb/adp/phase3_main/form

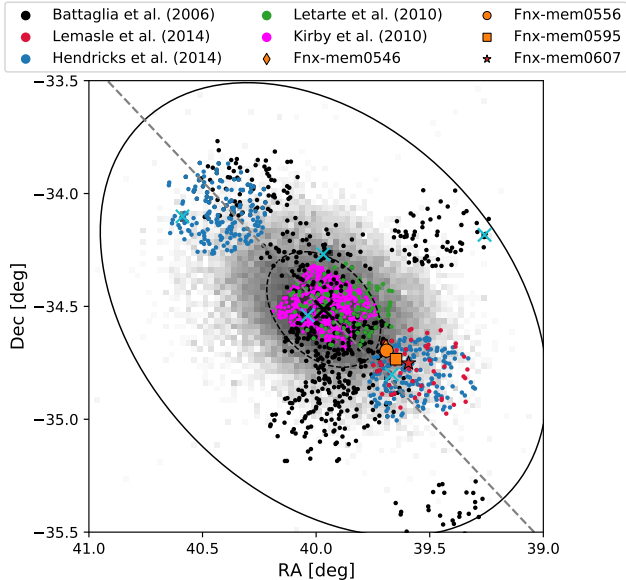


Figure 1. Coordinates of sample stars together with pointings of Battaglia et al. (2006), Lemasle et al. (2014), Hendricks et al. (2014), Letarte et al. (2010), and Kirby et al. (2010). The large oval shows the nominal tidal radius and the small dashed oval the core radius (Battaglia et al. 2006). The black cross marks the center of the galaxy as given by Battaglia et al. (2006). The grey 2D histogram shows the amount of stars observed by *Gaia* (DR2, Gaia Collaboration 2018a,b). Cyan crosses indicate the globular clusters of Fornax (Mackey & Gilmore 2003).

and KOA archives. More specifically, we assigned a star membership if its coordinates agree within a circle of three arcsec with the coordinates in the SIMBAD (Wenger et al. 2000), NED (NED Team 2007), or the second *Gaia* data release (DR2, Gaia Collaboration 2018a,b).

Therefore, the three Eu-enhanced stars are clearly members of Fornax as previous studies have already assigned them Fornax membership based on radial velocities, and distance to the centre of Fornax (see Fig. 1 and Battaglia et al. 2006; Lemasle et al. 2014). Also the proper motions of *Gaia* (DR2, Gaia Collaboration 2018a,b) indicate their membership (see Table 2).

The $[\alpha/\text{Fe}]$ ratio of the stars also fits with the general trend of Fornax (Fig. 2) and similar to many other r-process enriched metal-rich stars, a clear contribution from type Ia SNe is visible.

2.3. Stellar parameters

The stars were previously analysed by Lemasle et al. (2014), Reichert et al. (2020), and Battaglia et al. (2006). Table 3 shows their determined effective temperature, surface gravity, and metallicity (for Battaglia et al. 2006 the metallicities are from the calcium triplet).

Table 2. Proper motions in right ascension direction μ_δ , and in declination direction $\mu_\alpha \cos \delta$ taken from *Gaia* (DR2, Gaia Collaboration 2018a,b). Furthermore, we list the mean values of Fornax (McConnachie & Venn 2020).

Object	μ_δ [mas yr $^{-1}$]	$\mu_\alpha \cos \delta$ [mas yr $^{-1}$]
Fnx-mem0546	0.088 ± 0.145	-0.199 ± 0.210
Fnx-mem0556	0.400 ± 0.148	-0.775 ± 0.203
Fnx-mem0595	0.344 ± 0.120	-0.237 ± 0.167
Fornax (mean)	0.038 ± 0.003	-0.416 ± 0.004

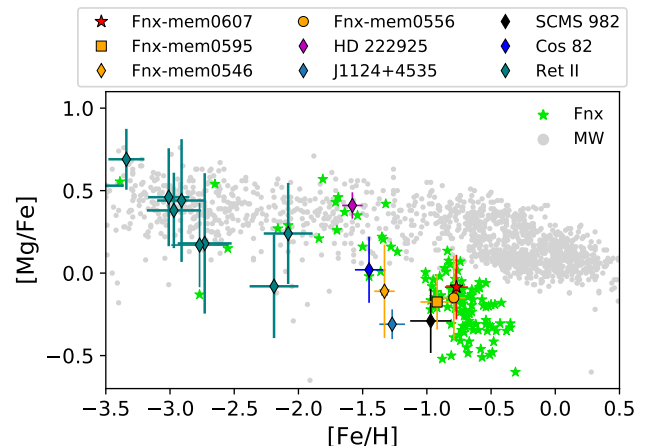


Figure 2. $[\text{Mg}/\text{Fe}]$ versus metallicity is shown for the four Fornax stars that we investigate here (see also Reichert et al. 2020): Fnx-mem0607 (red star), Fnx-mem0595 (yellow square), Fnx-mem0546 (yellow diamond), and Fnx-mem0556 (yellow circle). For comparison we show other Fornax stars (green stars, Reichert et al. 2020) and MW stars (grey dots, Reddy et al. 2003; Cayrel et al. 2004; Reddy et al. 2006; Ishigaki et al. 2013; Fulbright 2000; Nissen et al. 1997; Prochaska et al. 2000; Stephens & Boesgaard 2002; Ivans et al. 2003; McWilliam et al. 1995; Ryan et al. 1996; Gratton & Sneden 1988; Edvardsson et al. 1993; Roederer et al. 2016; Ezzeddine et al. 2020). Moreover, we compare to other typical r-process enhanced stars: Cos 82 (blue diamond, Shetrone et al. 2001), SCMS 982 (black diamond, Geisler et al. 2005), HD 222925 (magenta diamond, Roederer et al. 2018b), J1124+4535 (blue diamond, Xing et al. 2019), and Reticulum II (teal diamonds, Ji et al. 2016b). In all following figures we keep the same symbols and colors for the various stars.

We note that the star Fnx-mem0546 was excluded from Lemasle et al. (2014) due to convergence problems when determining the stellar parameters. Here, we adopt stellar parameters from Reichert et al. (2020). The effective temperatures and metallicities were derived using the automatic code SP_Ace (Boeche & Grebel 2016) which fits a theoretically calculated spectrum to the observed spectrum of the star until convergence is reached. The

theoretical spectrum is constructed by using a previously calculated curve of growth library. We note that the metallicity is therefore also biased by the LTE assumptions.

The surface gravities were derived using:

$$\log g_* = \log g_\odot + \log \frac{M_*}{M_\odot} + 4 \log \frac{T_{\text{eff},*}}{T_{\text{eff},\odot}} + 0.4 (M_{\text{bol},*} - M_{\text{bol},\odot}), \quad (1)$$

with $\log g_\odot = 4.44$, $T_{\text{eff},\odot} = 5780$ K, $M_* = 0.8 \pm 0.2 M_\odot$ and $M_{\text{bol},\odot} = 4.72$ mag, and the distance to Fornax of 147 ± 8 kpc taken from [Karczmarek et al. 2017](#)).

The microturbulence was calculated with an empirical relation from [Kirby et al. \(2010\)](#):

$$\xi_t = ((2.13 \pm 0.05) - (0.23 \pm 0.03) \cdot \log g) \text{ km s}^{-1}. \quad (2)$$

In general, effective temperatures in [Reichert et al. \(2020\)](#) are hotter than in [Lemasle et al. \(2014\)](#) because of the different methods in deriving them (spectroscopic versus photometric, see Appendix B of [Reichert et al. 2020](#) for a more detailed discussion). However, we stress that the strong neutron-capture element enhancement is also present when using the stellar parameters of [Lemasle et al. \(2014\)](#), hence the choice of stellar parameters does not change our conclusions.

3. ABUNDANCES

We combine the previously determined abundances ([Reichert et al. 2020](#)) with eight newly analyzed elements: Co, Zr, La, Ce, Pr, Nd, Er, and Lu (Table 4). Hyperfinesplitting is included for the redder lines of La, Co, and Lu ([Lawler & Dakin 1989](#); [Kurucz 2011](#)). We derive all additional abundances by synthesizing and fitting theoretical spectra with the local thermodynamic equilibrium (LTE) spectrum synthesis code MOOG (version of 2014, [Snedden 1973](#)) using 1-dimensional model atmospheres from [Kurucz \(1970\)](#)³, and solar abundances from [Asplund et al. \(2009\)](#). In addition, we have tried to extract carbon from several molecular absorption lines but those were too weak in the covered spectral region. Therefore, we can exclude a strong carbon enhancement.

All derived abundances, including those already obtained by [Reichert et al. \(2020\)](#), are presented in Table 5 for the four Fornax stars. The star Fnx-mem0607 is used as a reference because it has typical abundances of neutron-capture elements in Fornax stars. The stars Fnx-mem0556, and Fnx-mem0595 have the high-

est europium abundance ever observed to our knowledge with $\log \epsilon(\text{Eu}) = 0.98$ (Table 5). Within uncertainties, this is comparable only to SCMS 982 in Sculptor ($\log \epsilon(\text{Eu}) = 0.95 \pm 0.18$, [Geisler et al. 2005](#)). In the following, we will refer to them as Eu-stars, defining them as r-II stars (i.e., $[\text{Eu}/\text{Fe}] > 1$) at high metallicities (i.e., $[\text{Fe}/\text{H}] \gtrsim -1.5$).

The enhancement of neutron capture elements (Zr, Ba, and Eu) is evident from the spectra shown in Fig. 3, where we include also SCMS 982 ([Geisler et al. 2005](#)), a star with similar absolute europium abundances. All stars have similar stellar parameters and the strength of the lines can therefore be roughly compared (Fnx-mem0546 is slightly more metal-poor than the other stars). The europium absorption line is strongest for Fnx-mem0546, Fnx-mem0556, and Fnx-mem0595 and even comparable in strength to the nickel line close by. Note that SCMS 982 has stronger Ba and Zr lines than the Fornax stars indicating a considerable s-process or i-process enhancement of this Sculptor star (see Sect. 4.1).

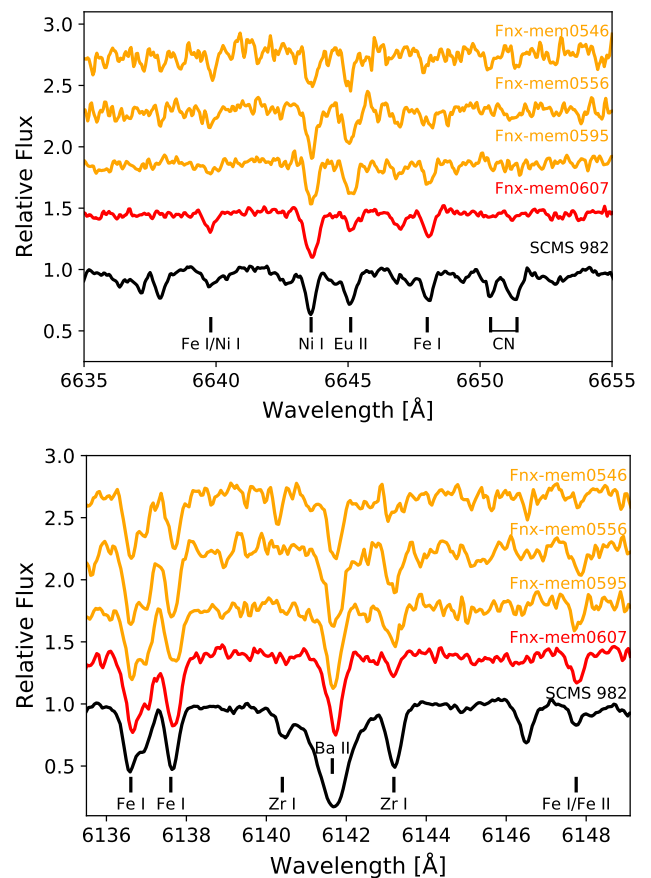


Figure 3. Spectra (including an offset for better visibility) for Fnx-mem0546, Fnx-mem0556, Fnx-mem0595, Fnx-mem0607, and SCMS 982 for regions around the Eu absorption line (top panel) and around a Ba II line (bottom panel).

³ <http://kurucz.harvard.edu/grids.html>

Table 3. Stellar parameters from different studies

Identifier	Reichert et al. (2020)			Lemasle et al. (2014)			Battaglia et al. (2006)
	T_{eff}	$\log g$	[Fe/H]	T_{eff}	$\log g$	[Fe/H]	[Fe/H]
Fnx-mem0546	4367 ± 110	0.82 ± 0.13	-1.33 ± 0.08	-	-	-	-1.31 ± 0.07
Fnx-mem0556	4176 ± 58	0.70 ± 0.12	-0.79 ± 0.09	3971 ± 150	0.64 ± 0.5	-0.63 ± 0.03	-0.64 ± 0.16
Fnx-mem0595	4223 ± 67	0.66 ± 0.12	-0.92 ± 0.13	3889 ± 150	0.51 ± 0.5	-0.88 ± 0.03	-1.04 ± 0.08
Fnx-mem0607	4207 ± 63	0.69 ± 0.12	-0.77 ± 0.09	3916 ± 150	0.55 ± 0.5	-0.96 ± 0.02	-

Table 4. Lines analyzed in addition to those used in Reichert et al. (2020).

Element	Wavelength	EP	$\log gf$	Literature
Co I	5483.34	1.709	-1.500	1
Y II	5509.89	0.992	-1.015	2
Zr I	6127.46	0.154	-1.060	3
Zr I	6134.62	0.000	-1.280	3
Zr I	6143.20	0.071	-1.100	3
La II	6320.43	0.173	-1.610	4
La II	6390.46	0.321	-1.410	5
Ce II	5512.08	1.007	-0.390	6
Pr II	5509.15	0.482	-1.168	7
Pr II	6165.94	0.923	-0.205	7
Nd II	5356.97	1.263	-0.280	8
Nd II	5361.17	0.559	-1.480	8
Nd II	5361.47	0.680	-0.370	7
Er II	5414.60	0.000	-2.499	7
Lu II	6221.87	1.540	-0.760	9

References—(1) Lawler et al. (2015); (2) Hannaford et al. (1982); (3) Biemont et al. (1981); (4) Corliss & Bozman (1962); (5) Lawler et al. (2001); (6) Lawler et al. (2009); (7) Meggers et al. (1975); (8) Den Hartog et al. (2003); (9) den Hartog et al. (1998).

In the following, we will compare the four Fornax stars to other stars keeping symbols and colors the same in all figures. Fnx-mem0546, Fnx-mem0556, Fnx-mem0595, Fnx-mem0607 (Reichert et al. 2020) are marked by an orange diamond, a circle, a square, and a red star, respectively. Other Fornax stars (Reichert et al. 2020) are shown as green stars, and the MW stars as grey dots (Reddy et al. (2003), Cayrel et al. (2004), Reddy et al. (2006), Ishigaki et al. (2013), Fulbright (2000), Nissen et al. (1997), Prochaska et al. (2000), Stephens & Boesgaard (2002), Ivans et al. (2003), McWilliam et al. (1995), Ryan et al. (1996), Gratton & Sneden (1988), Edvardsson et al. (1993), Roederer et al. (2016), Hansen et al. (2012) and Ezzeddine et al. (2020)). Moreover, we show other typical r-process enhanced stars: Cos 82 (blue diamond, Shetrone et al. 2001), SCMS 982 (black diamond, Geisler et al. 2005), HD 222925 (magenta di-

amond, Roederer et al. 2018b), J1124+4535 (blue diamond, Xing et al. 2019), and Reticulum II (teal diamonds, Ji et al. 2016b).

3.1. Largest Zr sample in a dwarf galaxy

We have derived (neutral) zirconium abundances for all Fornax stars presented in Reichert et al. (2020). For many stars it is the first Zr determination, making it the largest sample of Zr abundances in a dwarf galaxy to date. Figure 4 shows the [Zr/Fe] in Fornax including the neutron-capture enhanced stars. The average Zr abundance for all Fornax stars is slightly sub solar and the reference star (Fnx-mem0607) is located slightly below this general trend. There may be corrections to the abundances due to the LTE assumption which tends to affect neutral atoms more when they are the minority species as it is the case for Zr (c.f., Andrievsky et al. 2017, for a discussion). The exact size of the NLTE correction depends on several factors such as the stellar parameters and the abundance value. Currently, there is no large, available Zr NLTE grid covering our parameter space. However, based on NLTE computations in Velichko et al. (2010) and more recent ones in Hansen et al. (2020) we would estimate corrections of the order of ~ 0.0 to $> +0.3$ dex depending on the Zr abundances and stellar parameters. For our three enhanced stars the corrections would likely amount to $\gtrsim +0.3$ dex.

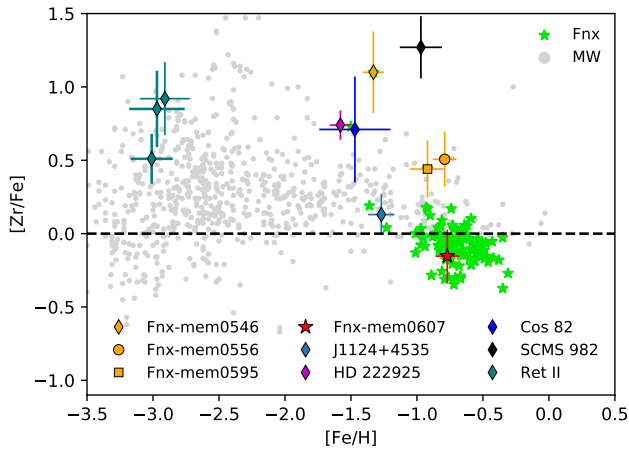
The three Eu-enhanced Fornax stars (Fnx-mem0546, Fnx-mem0556, and Fnx-mem0595) are clearly enhanced also in Zr. This agrees with these stars having an r-process pattern typical of other r-I or r-II stars, see for example the Reticulum II stars (teal diamonds) in Fig. 4 and the discussion in Sect. 4.1. Despite the high metallicities and Zr being dominated by the s-process in the solar system ($\sim 66\%$, Bisterzo et al. 2014); at low metallicities Zr is formed by the r-process as shown by most r-II stars. For the Eu-enhanced stars in Fornax, the enhancement of Zr is probably produced by an r-process event and not by the s-process, see Sect. 4.1.

3.2. Heavy neutron-capture elements

The three Eu-enhanced Fornax stars are enriched in europium with ~ 1 dex more than the average Fornax

Table 5. Derived absolute abundances (including also those already presented in Reichert et al. (2020, R20)).

Element	Fnx-mem0546	Fnx-mem0556	Fnx-mem0595	Fnx-mem0607	Reference
Mg I	6.16 ± 0.27	6.66 ± 0.24	6.51 ± 0.11	6.75 ± 0.17	R20
Sc I	1.26 ± 0.26	1.79 ± 0.10	1.60 ± 0.29	1.93 ± 0.11	R20
Ti II	3.93 ± 0.31	4.32 ± 0.25	3.79 ± 0.28	4.08 ± 0.11	R20
Cr I	3.57 ± 0.39	5.22 ± 0.26	4.76 ± 0.18	4.86 ± 0.44	R20
Mn I	3.90 ± 0.37	3.97 ± 0.14	4.15 ± 0.23	4.31 ± 0.28	R20
Fe I	6.17 ± 0.08	6.71 ± 0.09	6.58 ± 0.13	6.73 ± 0.09	R20
Co I	3.29 ± 0.29	3.90 ± 0.26	3.59 ± 0.24	3.93 ± 0.19	This study
Ni I	4.76 ± 0.20	5.14 ± 0.21	5.12 ± 0.23	5.11 ± 0.23	R20
Y II	0.89 ± 0.25	1.35 ± 0.29	1.11 ± 0.24	-	R20
Zr I	2.19 ± 0.30	2.29 ± 0.13	2.12 ± 0.18	1.70 ± 0.20	This study
Ba II	1.25 ± 0.12	1.76 ± 0.30	1.79 ± 0.14	1.65 ± 0.12	R20
La II	1.50 ± 0.28	1.47 ± 0.26	1.04 ± 0.13	0.60 ± 0.09	This study
Ce II	1.03 ± 0.25	1.33 ± 0.24	1.45 ± 0.24	-	This study
Pr II	1.17 ± 0.25	1.15 ± 0.34	1.01 ± 0.23	0.33 ± 0.15	This study
Nd II	1.49 ± 0.19	1.89 ± 0.29	1.82 ± 0.30	0.99 ± 0.22	This study
Eu II	0.64 ± 0.19	0.98 ± 0.13	0.98 ± 0.12	0.18 ± 0.34	R20
Er II	-	1.69 ± 0.25	1.53 ± 0.28	-	This study
Lu II	0.22 ± 0.23	0.61 ± 0.26	0.18 ± 0.37	< 0.23	This study
[Ba/Eu]	$-1.05 (r)$	$-0.88 (r)$	$-0.85 (r)$	$-0.19 (r + s)$	-
[Ba/La]	$-1.33 (r)$	$-0.80 (r)$	$-0.33 (r)$	$-0.03 (r + s)$	-

**Figure 4.** [Zr/Fe] versus metallicity following the same notation and references as in Fig. 2.

stars (see Fig. 5). With $\log \epsilon(\text{Eu}) = 0.98$, Fnx-mem0595 and Fnx-mem0556 are the most europium-enriched stars observed until today, together with SCMS 982 that is enriched by an s- or i- process (see Skúladóttir et al. 2020, for a discussion). Even though rare, there are several stars with enhanced europium at low metallicities. However, such stars are even more rare at high metallicities. In Fig. 5, we show some of those Eu-stars: Cos 82 (Shetrone et al. 2001; Aoki et al. 2007; Sadakane et al. 2004), J1124+4535 (Xing et al. 2019), HD 222925

(Roederer et al. 2018b), and SCMS 982 (Geisler et al. 2005; Skúladóttir et al. 2020). With the exception of SCMS 982, these stars show a dominant contribution from the r-process as indicated by their [Ba/Eu] ratio and discussed below (Fig. 7).

The combination of metal-rich stars together with the extreme enhancements of neutron capture elements gives us the unique possibility to derive abundances of neutron capture elements that are otherwise challenging to detect. Therefore, we are able to derive lutetium abundances (Fig. 6).

Due to the heavy blending of the absorption line, we claim a Lu detection if more than three points deviate by more than three sigma (dashed line in Fig. 6) from the flux when assuming basically no Lu (i.e., $[\text{Lu}/\text{H}] = -9$). Even though uncertain due to irregular noise next to the absorption line, we clearly detect lutetium in Fnx-mem0546, but also in Fnx-mem0556 and Fnx-mem0595. Because the continuum shows some artifacts next to the absorption line in Fnx-mem0595, we assign an additional error of 0.1 dex to the lutetium abundance. This adds all three stars to the rare stars with lutetium detections (9 in JinaBase, Abomalima & Frebel 2018, 13 in SAGA, Suda et al. 2017) and makes it the first detections in a dwarf spheroidal galaxy.

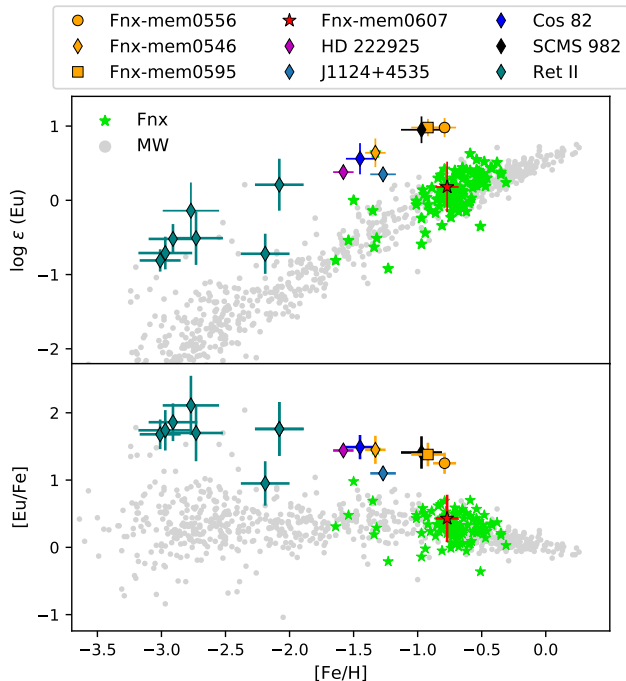


Figure 5. Absolute Eu (upper panel) and relative $[\text{Eu}/\text{Fe}]$ abundances (lower panel) versus metallicity following the same notation and references as in Fig. 2.

4. ORIGIN OF EU-STARS

In this section we probe the origin of the Eu-stars by first finding the predominant process that enriched these stars. Following, we assess which possible sites could host this process. We make use of yield predictions and abundance ratios for this purpose, but we caution the use of a single element ratio to assign a dominant process contribution. We point towards using such ratios together with observationally derived abundance patterns, as these present a more complete chemical trace of the true stellar enrichment.

4.1. *r*-, *i*-, or *s*-process?

At high metallicity, the neutron-capture elements stem mainly from the *s*- and *r*-process, possibly also from the *i*-process. The *i*-process operates at intermediate *n*-densities and exposures and may be able to take place in rapidly accreting white dwarfs (e.g., Denissenkov et al. 2017), super asymptotic giant branch stars (e.g., Doherty et al. 2015), or low-mass AGB (e.g., Stancliffe et al. 2011). In order to check whether the Eu-stars are enriched by an *r*-process event or whether they have a strong contribution from the *s*-process, we first check the $[\text{Ba}/\text{Eu}]$ ratio shown in Fig. 7 and Table 5. For the three stars, the ratio is well below zero and this is often used to define neutron-capture-rich, *r*-process enhanced stars ($[\text{Ba}/\text{Eu}] < 0$, Beers & Christlieb 2005). A stronger

constraint on the heavy-element enhancement is the estimate of the pure process trace, which is typically assessed through the $[\text{Ba}/\text{Eu}]$ being less than ~ -0.7 dex (pure *r*) or larger than ~ 1.1 dex (pure *s*) (Arlandini et al. 1999; Hansen et al. 2018). The $[\text{Ba}/\text{Eu}]$ ratio points towards a pure *r*-ratio in the three Fornax stars, while the reference star, Fnx-mem0607, is clearly a mixture of *r* and *s*.

We also probe if there is an *i*-process contamination. A typical fingerprint of the *i*-process is a positive $[\text{Ba}/\text{La}]$ ratio (Koch et al. 2019; Hampel et al. 2016; Denissenkov et al. 2019), but this ratio is negative for the four Fornax stars. In this connection, we note that Fnx-mem0546 has a relatively low Ba abundance with respect to La and also compared to the Ba in the other two stars. The La abundance is more than 1 dex higher than the Ba abundance in Fnx-mem0546. This leads to a strong odd-even abundance difference in this region. In Fig. 7, it is also clear that SCMS 982 is not *r*-process dominated with $[\text{Ba}/\text{Eu}]$ close to 0.5. If the peculiar pattern of SCMS 982 stems from an *s*- or *i*-process is still under debate (Geisler et al. 2005; Skúladóttir et al. 2020). Based on these abundance ratios, we focus our further comparison on *r*-process and *s*-process yields.

We now compare the observationally derived abundances to theoretical predictions. For the *s*-process, we take yields for different AGB star masses and metallicities from the F.R.U.I.T.Y. database (Cristallo et al. 2011, 2015). In Fig. 7, this contribution is shown by horizontal dashed and dotted lines covering the metallicity range where they are predicted and appropriate. For the *r*-process, we compare to yields from different scenarios (for details see Sect. 4.3). The variation in any abundance ratio within a given scenario is due to the nuclear physics uncertainties (see Côté et al. 2021; Eichler et al. 2019, for more details about models and nuclear physics included in the nucleosynthesis). As seen from Fig. 7, the $[\text{Ba}/\text{Eu}]$ ratios of the three Eu-stars agree with the theoretical predictions of the *r*-process within uncertainties. However, those uncertainties are rather large and thus it is not possible to conclude which scenario contributed most to the observed abundances.

Now we explore another possibility to check whether the three Eu-star’s abundances are mainly due to the *r*-process. We compare their abundance patterns to that of HD 222925 (Roederer et al. 2018b), a star that has been identified as *r*-process enhanced. Figure 8 shows this comparison and demonstrates that two of the Eu-stars (Fnx-mem0556 and Fnx-mem0595) fit with an excellent reduced $\chi^2 < 1$ the *r*-process pattern of HD 222925. Fnx-mem0546 deviates slightly from this pattern with an enhancement in lanthanum,

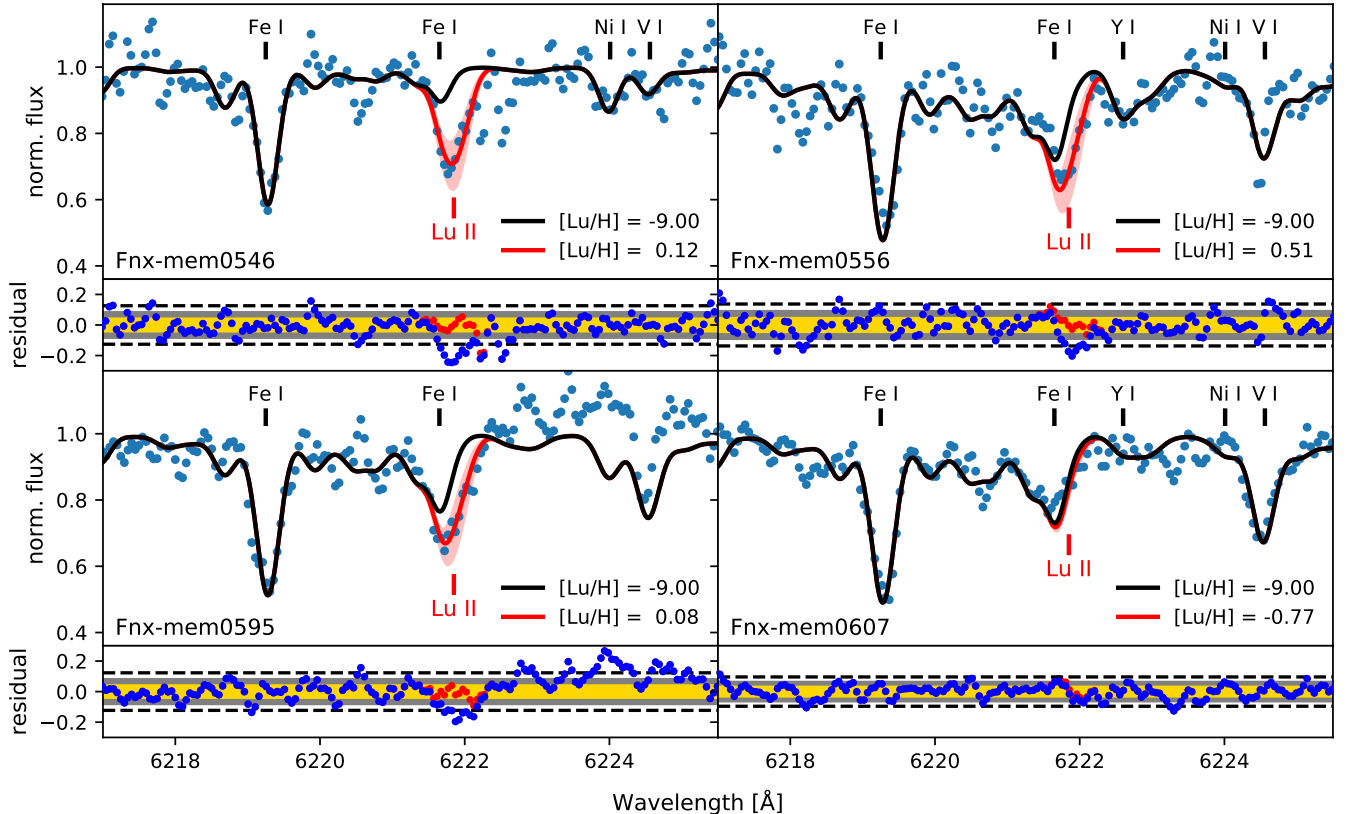


Figure 6. Normalized flux together with a synthetic spectrum. The synthetic spectrum is shown for a negligible amount of Lu (black line) and for an enhanced Lu abundance (red line). A red band indicates a deviation of the Lu abundance in the range of a typical error (± 0.3 dex). The lower panels show the residual of the synthetic spectrum with respect to the observed flux. Yellow horizontal bands mark a one sigma deviation from the synthesized spectra, grey bands a two sigma deviation, and dashed lines a three sigma deviation.

and praseodymium relative to barium and europium. Lutetium on the other hand agrees well with the r-process pattern for Fnx-mem0546 and Fnx-mem0556. For Fnx-mem0595, lutetium is underabundant compared to the r-process ratio, however, it also has a larger error (see Sect. 3.2). In summary, all stars show a striking similarity to the r-process pattern without too many contributions from other processes. We can therefore safely assume that the abundances of the three Eu-stars are mainly enriched by the r-process.

4.2. One r-process event

After showing that the Eu-stars are r-process enhanced, we estimate how many r-process events are necessary to enrich these stars and calculate the ejected europium per event. The three Eu-stars were born in a gas cloud/region with a total mass M_{gas} . Magg et al. (2020) provide an approximation for the dilution mass where the new elements from an r-process event(s) are mixed:

$$M_{\text{gas}} = 1.9 \cdot 10^4 M_{\odot} E_{51}^{0.96} n_0^{-0.11}, \quad (3)$$

here n_0 is the ambient density and E_{51} is the explosion energy of the event. Magg et al. (2020) uses $n_0 = 1$ corresponding to the environment where Pop III stars formed, however this has a small impact on the final dilution mass due to the small exponent. The explosion energy (E_{51}) of the event can be assumed to be between 10^{51} and 10^{52} erg (c.f., 10^{51} erg for GW170817; Kathirgamaraju et al. 2019 and the explosion energy of 10^{52} erg of hypernovae; Nomoto et al. 2006). The dilution mass (M_{gas}) therefore lies between 10^4 to $10^5 M_{\odot}$, which is at least three orders of magnitudes smaller than the total stellar mass of Fornax $M_{\text{Fornax}} \sim 10^8 M_{\odot}$ (Lokas 2009).

Before the r-process event(s), the mass of Eu in the gas was $M_{\text{Eu}}^{\text{pre-event}}$ and the mass injected by the event was $M_{\text{Eu}}^{\text{r-event}}$. We can estimate $M_{\text{Eu}}^{\text{pre-event}}$ using the abundance of our reference star, Fnx-mem0607, in the following definition:

$$\log \epsilon(\text{Eu}) = \log \frac{M_{\text{Eu}}^{\text{pre-event}}}{A_{\text{Eu}} \cdot M_{\text{gas}}} + 12, \quad (4)$$

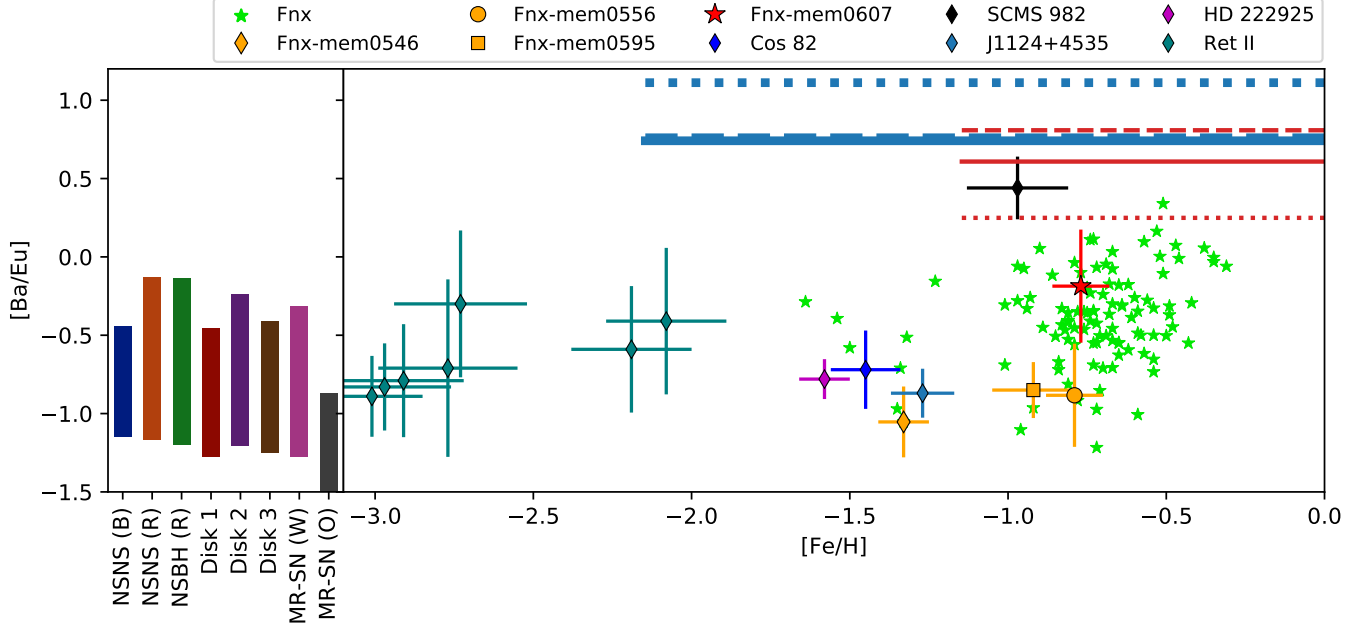


Figure 7. [Ba/Eu] versus metallicity (right panel) following the same notation and references as in Fig. 2. Theoretical predictions are shown for s-process (horizontal lines) and r-process (left panel). The s-process yields are from F.R.U.I.T.Y. database (Cristallo et al. 2011) and are indicated by horizontal lines starting at the metallicity of the model. These models are for three AGB masses: $1.3 M_{\odot}$ (solid lines), $2.0 M_{\odot}$ (dashed lines), and $5.0 M_{\odot}$ (dotted lines). The red, thin lines indicate a metallicity of $Z = 0.001$, and blue, thick lines correspond to $Z = 0.0001$ and $[\alpha, \text{Fe}] = 0.5$. The r-process ratios are shown with bars that cover the calculate range taking into account uncertainties due to the various astrophysical conditions and different nuclear physics theoretical models. The ratio is shown for the early, dynamical ejecta of neutron star merger (NSNS) and neutron star black hole merger (NSBH) as well as for their disk ejecta (Disk 1, Disk 2, and Disk 3). Results are also presented for MR-SNe based on two simulations. For more details and references see Sect. 4.3 and Côté et al. (2021); Eichler et al. (2019); Reichert et al. (2021).

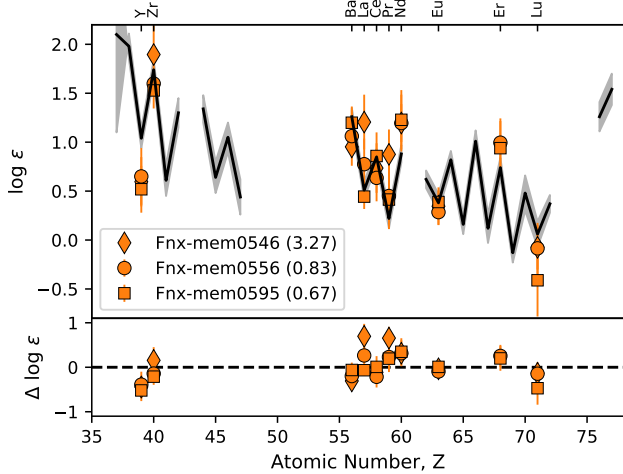


Figure 8. Abundances of Fnx-mem0546 (diamonds), Fnx-mem0556 (circles), and Fnx-mem0595 (squares) scaled to fit the r-process pattern of HD 222925 (black line, with errors indicated as grey bands, Roederer et al. 2018b). In the legend we give the reduced χ^2 of the fit for $Z > 50$. Bottom panel shows the relative differences between the Fornax stars and HD 222925.

where $A_{\text{Eu}} = 152$ is the average mass number of europium. Therefore, the Eu in the r-process stars is:

$$\log \epsilon(\text{Eu}) = \log \frac{M_{\text{Eu}}^{\text{pre-event}} + M_{\text{Eu}}^{\text{r-event}}}{A_{\text{Eu}} \cdot M_{\text{gas}}} + 12, \quad (5)$$

and from this expression we obtain an europium mass per event $M_{\text{Eu}}^{\text{r-event}}$ between $\sim 1.5 \cdot 10^{-5}$ and $\sim 3 \cdot 10^{-4} M_{\odot}$. This is similar to the values reported by Ji et al. (2016a) to explain the r-process enhanced stars in Reticulum II ($\sim 2.5 \cdot 10^{-5} - 5 \cdot 10^{-5} M_{\odot}$). Therefore, it is likely that Fnx-mem0556, Fnx-mem0595, and Fnx-mem0546 also got enriched by a single r-process event. Moreover, the stars probably formed only a few Myr after the event. Otherwise, the r-process material would have been mixed into a larger amount of gas (van de Voort et al. 2020).

Our simple estimate has several input parameters (e.g., n_0 , E_{51}), therefore we show in Fig. 9 an overview covering different possible values. In this figure, the absolute europium abundances of Fnx-mem0556 are indicated by horizontal orange lines, the estimated dilution mass by vertical orange lines, and the colors correspond to the Eu mass ejected by the r-process event using

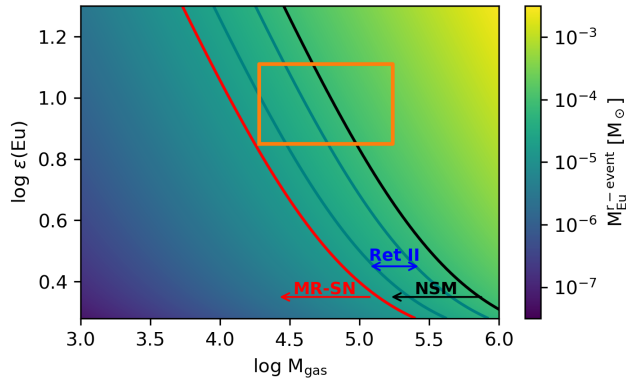


Figure 9. Absolute abundances of europium versus dilution mass. The amount of europium needed to enhance a star to a given absolute abundance value is color coded. The orange box indicates the range, predicted from Fnx-mem0556, where the left and right vertical lines are obtained from different explosion energies and the horizontal lines from the observed absolute europium abundances including the error. The range of estimated Eu masses to enhance Reticulum II (Ji et al. 2016a) is given by blue lines. The maximum Eu mass ejected from NSMs based on simulation is shown as a black line ($8 \cdot 10^{-5} M_{\odot}$), while the maximum ejected europium mass from MR-SNe simulations is traced by red line ($1.5 \cdot 10^{-5} M_{\odot}$).

Eq. 5. The latter changes smoothly over several orders. However, the amount of Eu needed to explain the Eu-stars ($M_{\text{Eu}} \sim 10^{-5} - 10^{-4} M_{\odot}$, Fig. 9) agrees with having only one r-process event (c.f. also Beniamini et al. 2016 for estimates of the ejected Eu mass per r-event in dSph galaxies.).

4.3. Chasing the r-process site in Fornax

Which r-process event is responsible for the enhanced Eu in the three Fornax stars? The possible candidates are compact binary mergers (two neutron stars or a neutron star and a black hole) and MR-SNe including the early explosion phase and the late evolution as collapsar.

In Fig. 7, we have compared the [Ba/Eu] of the Eu-stars to various theoretical predictions from compact binary mergers (dynamical and disk ejecta) and from MR-SNe using different nuclear physics input (Kodama & Takahashi 1975; Duflo & Zucker 1995; Panov et al. 2001; Möller et al. 2003; Kelic et al. 2008; Marketin et al. 2016). We test the dynamical ejecta of mergers of two neutron stars (NSNS (B), Bovard et al. 2017) and (NSNS (R), Korobkin et al. 2012), and a neutron star and a black hole (NSBH (R), Korobkin et al. 2012); ejecta from the accretion disk formed after merger surrounding the compact object (Disk 1, Disk 2, and Disk 3, Wu et al. 2016); ejecta from magneto-rotational supernovae MR-SN (W) (Winteler et al. 2012) and MR-SN (O) (Re-

ichert et al. 2021). A similar set of models was used also by Côté et al. (2021); Eichler & Arcones (2021) to compare to meteorite ratios of r-process isotopes. However, there are too large theoretical uncertainties in the nuclear physics input as well as the variation in the astrophysical conditions and this makes it impossible to conclude from the [Ba/Eu] ratio alone which scenario has contributed to the enhanced Eu.

The mass of Eu estimated above ($M_{\text{Eu}} \sim 10^{-5} - 3 \cdot 10^{-4} M_{\odot}$) could be also used as a constraint on the r-process site. We compare this amount of Eu to the mass that is ejected in NSM and MR-SNe, as obtained in hydrodynamic simulations. However, these simulations are still uncertain due to various aspects (e.g., resolution, magnetic fields, neutrino matter interactions, high density equation of state) and predictions about the amount of Eu ejected are only approximate.

In compact binary mergers, the masses of ejected europium in the dynamic ejecta depends on the simulation and can differ by orders of magnitudes (see, e.g., Côté et al. 2018 for an overview of different ejecta masses of the dynamical ejecta). Just to name a few examples, the europium mass based on the simulation of Bovard et al. (2017) is $M_{\text{Eu}} \sim 10^{-6} - 10^{-5} M_{\odot}$. Yields of other simulations are slightly higher with $M_{\text{Eu}} \sim 10^{-5} - 8 \cdot 10^{-5} M_{\odot}$ (Korobkin et al. 2012) and similar $M_{\text{Eu}} \sim 3 \cdot 10^{-5} - 5 \cdot 10^{-5} M_{\odot}$ (Goriely et al. 2011). In the case of a NSBH merger, the ejected europium mass of the dynamic ejecta can reach $M_{\text{Eu}} \sim 3 \cdot 10^{-4} M_{\odot}$ (Korobkin et al. 2012). In addition, the disk ejecta will also contribute to europium ($M_{\text{Eu}} \sim 3 \cdot 10^{-6} - 10^{-5} M_{\odot}$, Wu et al. 2016). However, it is still under discussion how much each ejected component contributes and how neutron-rich the components are (see, e.g., Shibata & Hotokezaka 2019, for a recent review).

In GW170817, Watson et al. (2019) directly observed Sr and predicted a mass $M(\text{Sr}) \gtrsim 5 \cdot 10^{-5} M_{\odot}$. When assuming that the ejecta is scaled like the solar r-process residual (Snedden et al. 2008) the ejected europium mass is $M_{\text{Eu}} \sim 3 \cdot 10^{-6} M_{\odot}$. We note that the lighter heavy elements like strontium usually scatter with respect to the heavier elements. Because of this and other involved uncertainties, this value should be treated as a rough estimate only. Nevertheless, it agrees well with the masses of $M_{\text{Eu}} \sim 3 \cdot 10^{-6} - 1.5 \cdot 10^{-5} M_{\odot}$ obtained in Côté et al. (2018) for GW170817.

The amount of Eu produced in MR-SNe based on recent simulations is $\lesssim 1 \cdot 10^{-5} M_{\odot}$ (Winteler et al. 2012), $\lesssim 1.5 \cdot 10^{-5} M_{\odot}$ (Nishimura et al. 2015), $\lesssim 8 \cdot 10^{-6} M_{\odot}$ (Nishimura et al. 2017), and $\lesssim 5 \cdot 10^{-6} M_{\odot}$ (Reichert et al. 2021). These values are on the lower end of our assumed uncertainties (Fig. 9), but they could still be

responsible for the enrichment. After some MR-SNe, a black hole forms and is surrounded by an accretion disk. The disk conditions may be similar to those found in accretion disks after neutron star mergers and may favour an r-process. Siegel et al. (2019) have found that Eu may be produced in collapsars, however, more detailed investigations are necessary to understand whether the conditions are appropriate for an r-process, see Miller et al. (2020); Just et al. (2021).

In Fig. 9, we show the maximum europium mass ejected by NSM (black line, $8 \cdot 10^{-5} M_{\odot}$) and by MR-SNe (red line, $1.5 \cdot 10^{-5} M_{\odot}$). Moreover, we include the estimated europium mass necessary to explain r-II stars in Reticulum II (Ji et al. 2016a). All of these estimates are close to the mass that is necessary to enhance the Eu-stars, as derived from the observed stellar abundances.

In addition to Eu, one can use α -elements, e.g., Mg, to check whether MR-SNe are the r-process site responsible for more element abundances in the Fornax Eu-stars. Since the amount of ejected α -elements depends on the progenitor mass (e.g., Kobayashi et al. 2006), and the progenitors of MR-SNe may differ from the average CC-SNe, the amount of ejected α -elements may also vary between the two types of SNe. If an abnormal supernova produces r-process material and a huge amount of Mg, one would possibly see a signature of this in the Mg abundances in the Fornax Eu-stars. However, in Fig. 2, the three stars present normal Mg abundances (see also Table 5). This may be an indication of a neutron star merger producing the observed Eu or of MR-SNe ejecting normal amount of Mg as any other supernova in Fornax. Therefore, we cannot use Mg as an indicator for rare supernovae and their r-process yields.

In summary, based on the abundance ratio of [Ba/Eu], on the estimated amount of Eu, and on the Mg abundance, we cannot determine the r-process site enriching the Eu-stars in Fnx. Based on Fig. 9, NSMs seem a promising site to explain the r-material in the Eu-stars, however, their time delay coupled with recent star formation in Fnx may pose an issue that is easier to overcome if MR-SNe would be the r-site. On the other hand, recent studies also show that a substantial fraction of the NSM population may occur on short timescales (< 100 Myr, see e.g. Beniamini & Piran 2019).

4.4. Time scale - late r-process event linked to a star formation burst in Fornax

The strong r-process enhancement, despite the remaining unknown formation site, combined with the typical low α -content indicates, together with the *Gaia* proper motions (DR2, Gaia Collaboration 2018a,b), that

these rare Eu-stars are indeed Fornax members (see Sect. 2.2).

From the time scale perspective, neutron star mergers remain viable sources and could explain the observed abundances. Neutron star mergers are expected to contribute with some delay and thus such an event could account for producing r-process material late or at high metallicities. However, this would imply that there is some star formation just after the neutron stars merge and eject r-process material. Similarly linked to the late star formation, massive stars could also have formed and exploded as MR-SNe producing the r-process observed in the Eu-stars. This would require more gas at a later stage, which may be feasible in Fornax. In any case, the three r-rich stars must have formed shortly after the r-process event, i.e., there must have been an active star forming environment. According to Lemasle et al. (2014), Fnx-mem0556 has an age of 4.36 ± 0.86 Gyr and Fnx-mem0595 an age of 5.75 ± 1.78 Gyr. Fornax shows a complex star formation history with several outbreaks. A significant number of stars were formed at early times, i.e., more than 10 Gyr ago. Moreover, there was a very recent period of star formation ~ 4 Gyr ago (e.g., Coleman & de Jong 2008; de Boer et al. 2012; Hendricks et al. 2014; Weisz et al. 2014; Rusakov et al. 2021). This late sudden burst of star formation agrees well with the age of the r-process enhanced stars. Although the origin of this burst is not known, there are speculations that Fornax has undergone some galaxy merger events in its history, indicated by over-dense features in the spatial distribution of stars in Fornax (e.g., Coleman et al. 2004).

Another explanation for such an peculiar enhancement of neutron-capture elements was investigated by Tsujimoto & Shigeyama (2002). They proposed that inhomogeneous mixing, caused by a high velocity dispersion in dSph galaxies may be responsible for the existence of stars as Cos 82, and possibly also Fnx-mem0546, Fnx-mem0556, and Fnx-mem0595 (see also Sadakane et al. 2004; Aoki et al. 2007, for a discussion).

5. CONCLUSIONS

We study neutron-capture elements in Fornax stars including three stars at high metallicities with extreme enhancements of heavy r-process elements. We define these new type of stars as Eu-stars, they are r-II stars ($[\text{Eu}/\text{Fe}] > 1$) at high metallicity ($[\text{Fe}/\text{H}] \gtrsim -1.5$). Although previously observed, metal-rich stars with enhanced neutron-capture elements are rare. The Eu-stars show an europium abundance up to $\log \epsilon(\text{Eu}) = 0.98 \pm 0.12$, which is the highest europium abundance ever observed. Thus, Eu is approximately three times

more abundant than in our Sun while their iron abundance is a factor of seven smaller. In addition to an enrichment in heavy neutron-capture elements, Zr is also enhanced in the three stars. In order to compare to other Fornax stars, we have derived Zr abundances for 105 stars. This is the largest Zr sample in a dSph to date and offers a new chance to explore the galactic chemical evolution of Fornax. Moreover, we have derived lutetium abundances for the first time for stars in a dSph galaxy. This was possible due to the unique combination of high metallicities and r-process enrichment that allowed for a Lu line detection.

We have demonstrated that the enhancements in neutron-capture elements is due to the r-process as indicated by the [Ba/Eu] ratio and typical r-process pattern. Moreover, we give an estimate of the amount of Eu necessary to explain these r-process rich / Eu-stars, namely $M(\text{Eu}) \sim 8 \cdot 10^{-6} - 3 \cdot 10^{-4} M_{\odot}$. This agrees with an individual r-process event being enough to explain the observed Eu abundances. Based on the elemental ratios and the europium mass ejected, we try to identify the r-process site by comparing to theoretical yield predictions from neutron star mergers and magneto-rotational supernovae. However, the uncertainties in the astrophysical conditions and the nuclear physics input prevent us of making any firm conclusion about the site. There is a clear need of improved hydrodynamic simulations with detailed microphysics as well as more theoretical and experimental information of the extreme neutron-rich nuclei involved in the r-process.

The r-process event responsible for the Eu-stars was occurring during a star formation episode. If the event was a NSM, this could come from neutron stars born in early supernovae. The delay of the merger was coinciding with the star formation event where the Eu-stars were born shortly after. Despite NSM yield a very promising range of Eu abundances, the time scale is a

bit more tricky in this scenario. Another possibility is that during the star formation event, massive stars formed and at least one died fast as a MR-SN ejecting the r-process material necessary to explain the observed abundances. Therefore, an active star forming environment simultaneously with the r-process event is in any case required for the formation of stars with such an enhanced europium content. The age of the stars approximately traces the time when the r-process event occurred. Their age is estimated to be around 4 Gyr (Lemasle et al. 2014), which coincides with a sudden increase of star formation in Fornax (Coleman & de Jong 2008; de Boer et al. 2012; Hendricks et al. 2014; Weisz et al. 2014; Rusakov et al. 2021). We conclude that the existence of these Eu-stars proves that the r-process can efficiently form r-II stars across a broad range of dwarf galaxies - from the faintest low-mass ones to the most massive dSph galaxies. It is not unique to ultra faint dwarf galaxies as suggested before. Moreover, we emphasize that gas dilution and star formation time scales must be considered in the search for the r-process sites. Future observations are critical to find more Eu-stars that are key to understand the origin of heavy elements produced by the r-process.

ACKNOWLEDGMENTS

The authors thank M. Eichler, M. Hanke, A. Koch, and Á. Skúladóttir for valuable discussions. MR and AA were supported by the ERC Starting Grant EUROPIUM-677912, Deutsche Forschungsgemeinschaft through SFB 1245, and Helmholtz Forschungsakademie Hessen für FAIR. CJH acknowledges support from the Max Planck Society. This work has benefited from the COST Action “ChETEC” (CA16117) supported by COST (European Cooperation in Science and Technology).

APPENDIX

A. ZIRCONIUM ABUNDANCES

We list all derived zirconium abundances together with metallicities from Reichert et al. (2020) in Table 6.

REFERENCES

- Abbott, B. P., Abbott, R., Abbott, T. D., et al. 2017, *Phys. Rev. Lett.*, 119, 161101, doi: [10.1103/PhysRevLett.119.161101](https://doi.org/10.1103/PhysRevLett.119.161101)
- Abohalima, A., & Frebel, A. 2018, *ApJS*, 238, 36, doi: [10.3847/1538-4365/aadfe9](https://doi.org/10.3847/1538-4365/aadfe9)
- Andrievsky, S. M., Korotin, S. A., Hill, V., & Zhukova, A. V. 2017, *Odessa Astronomical Publications*, 30, 54, doi: [10.18524/1810-4215.2017.30.117154](https://doi.org/10.18524/1810-4215.2017.30.117154)
- Aoki, W., Honda, S., Sadakane, K., & Arimoto, N. 2007, *PASJ*, 59, L15, doi: [10.1093/pasj/59.3.L15](https://doi.org/10.1093/pasj/59.3.L15)

Table 6. Metallicities and zirconium abundances of 105 stars in Fornax.

ID	[Fe/H]	$\log \epsilon(\text{Zr})$	ID	[Fe/H]	$\log \epsilon(\text{Zr})$
[LHT2010] BL147	-1.50 ± 0.05	1.81 ± 0.22	[WMO2009] For-0956	-0.72 ± 0.08	1.81 ± 0.17
[WMO2006] F01-20	-1.36 ± 0.05	1.41 ± 0.11	2MASS J02384113-3444205	-0.71 ± 0.05	1.57 ± 0.13
[LDH2014] Fnx-mem0546	-1.33 ± 0.08	2.35 ± 0.27	2MASS J02401677-3429346	-0.71 ± 0.07	1.80 ± 0.13
[WMO2009] For-0970	-1.23 ± 0.05	1.39 ± 0.11	[MOW91] 8	-0.70 ± 0.10	1.75 ± 0.13
[WMO2009] For-0361	-1.01 ± 0.11	1.57 ± 0.19	[LDH2014] Fnx-mem0715	-0.70 ± 0.13	1.77 ± 0.18
2MASS J02401043-3425177	-1.01 ± 0.10	1.44 ± 0.10	[WMO2009] For-0391	-0.69 ± 0.07	1.90 ± 0.15
[WMO2009] For-1877	-0.97 ± 0.09	1.53 ± 0.13	2MASS J02383503-3441380	-0.69 ± 0.06	1.83 ± 0.22
[LDH2014] Fnx-rgb0553	-0.97 ± 0.05	1.64 ± 0.14	2MASS J02390157-3436488	-0.68 ± 0.08	1.68 ± 0.12
[WMO2009] For-0968	-0.96 ± 0.06	1.61 ± 0.20	2MASS J02395144-3421211	-0.68 ± 0.09	1.84 ± 0.22
[MOW91] 25	-0.95 ± 0.09	1.60 ± 0.16	[LDH2014] Fnx-mem0574	-0.67 ± 0.05	1.90 ± 0.18
[LHT2010] BL100	-0.94 ± 0.10	1.55 ± 0.14	2MASS J02391102-3428348	-0.67 ± 0.10	1.86 ± 0.15
GB07 Fnx11	-0.93 ± 0.06	1.83 ± 0.14	2MASS J02390031-3430302	-0.67 ± 0.05	1.62 ± 0.14
[LDH2014] Fnx-mem0595	-0.92 ± 0.13	2.10 ± 0.15	[LDH2014] Fnx-mem0638	-0.67 ± 0.07	1.60 ± 0.15
[LDH2014] Fnx-mem0675	-0.92 ± 0.11	1.83 ± 0.19	[LDH2014] Fnx-mem0631	-0.67 ± 0.08	1.76 ± 0.13
[WMO2009] For-1579	-0.90 ± 0.06	1.80 ± 0.14	2MASS J02401790-3427010	-0.67 ± 0.07	1.93 ± 0.18
2MASS J02392805-3434013	-0.89 ± 0.08	1.41 ± 0.13	[WMO2009] For-0365	-0.65 ± 0.06	1.78 ± 0.12
[LDH2014] Fnx-mem0629	-0.88 ± 0.05	1.68 ± 0.20	2MASS J02401752-3426065	-0.65 ± 0.09	1.89 ± 0.15
2MASS J02385721-3435400	-0.86 ± 0.08	1.72 ± 0.15	[KGS2010] For 64059	-0.65 ± 0.10	1.82 ± 0.20
2MASS J02392022-3431571	-0.85 ± 0.07	1.72 ± 0.14	[WMO2009] For-0387	-0.65 ± 0.11	1.93 ± 0.14
[WMO2009] For-1219	-0.84 ± 0.06	1.78 ± 0.14	2MASS J02385365-3433048	-0.64 ± 0.08	1.81 ± 0.13
2MASS J02394528-3431581	-0.84 ± 0.04	1.66 ± 0.17	[WMO2009] For-0910	-0.64 ± 0.05	2.00 ± 0.22
[LDH2014] Fnx-mem0626	-0.83 ± 0.07	1.64 ± 0.11	2MASS J02391606-3430135	-0.62 ± 0.08	2.01 ± 0.12
2MASS J02393153-3423052	-0.83 ± 0.11	1.66 ± 0.14	2MASS J02390853-3430556	-0.62 ± 0.07	1.95 ± 0.12
[LHT2010] BL158	-0.82 ± 0.07	1.81 ± 0.19	2MASS J02395427-3435114	-0.61 ± 0.11	1.94 ± 0.20
2MASS J02383502-3442406	-0.81 ± 0.06	1.86 ± 0.22	2MASS J02391398-3428364	-0.60 ± 0.11	1.81 ± 0.12
GB07 Fnx08	-0.81 ± 0.05	1.74 ± 0.16	[LDH2014] Fnx-mem0682	-0.59 ± 0.06	1.89 ± 0.12
[LHT2010] BL204	-0.81 ± 0.03	1.69 ± 0.12	[LDH2014] Fnx-mem0717	-0.59 ± 0.08	1.78 ± 0.18
[LHT2010] BL261	-0.81 ± 0.11	1.51 ± 0.17	2MASS J02391437-3434427	-0.59 ± 0.09	2.09 ± 0.17
[LDH2014] Fnx-mem0633	-0.81 ± 0.12	1.65 ± 0.20	[LDH2014] Fnx-mem0678	-0.58 ± 0.07	1.93 ± 0.22
2MASS J02391159-3430448	-0.79 ± 0.07	1.68 ± 0.12	2MASS J02391783-3430570	-0.57 ± 0.10	1.90 ± 0.15
[LDH2014] Fnx-mem0634	-0.79 ± 0.08	1.48 ± 0.19	[WMO2009] For-1581	-0.57 ± 0.08	1.83 ± 0.29
[WMO2009] For-2280	-0.79 ± 0.05	1.77 ± 0.17	[LHT2010] BL233	-0.56 ± 0.12	1.83 ± 0.17
[LDH2014] Fnx-mem0556	-0.79 ± 0.09	2.30 ± 0.17	[WMO2009] For-2026	-0.54 ± 0.06	1.90 ± 0.13
[LHT2010] BL084	-0.78 ± 0.10	1.70 ± 0.19	2MASS J02393808-3437062	-0.54 ± 0.08	1.90 ± 0.15
[WMO2006] F01-23	-0.78 ± 0.06	1.62 ± 0.11	[WMO2009] For-1120	-0.54 ± 0.08	2.00 ± 0.13
[LDH2014] Fnx-mem0607	-0.77 ± 0.09	1.66 ± 0.16	2MASS J02394195-3430361	-0.54 ± 0.06	2.00 ± 0.14
[LDH2014] Fnx-mem0572	-0.77 ± 0.04	1.78 ± 0.21	2MASS J02384018-3439121	-0.53 ± 0.07	1.96 ± 0.19
2MASS J02390434-3425190	-0.76 ± 0.04	1.66 ± 0.12	2MASS J02390819-3436537	-0.52 ± 0.08	1.93 ± 0.15
[LDH2014] Fnx-mem0532	-0.76 ± 0.11	1.52 ± 0.25	2MASS J02392769-3437487	-0.51 ± 0.08	2.01 ± 0.12
[LDH2014] Fnx-mem0543	-0.75 ± 0.10	1.66 ± 0.13	2MASS J02395604-3424106	-0.51 ± 0.06	2.01 ± 0.13
[LHT2010] BL311	-0.75 ± 0.04	1.78 ± 0.19	2MASS J02392483-3434383	-0.50 ± 0.05	2.00 ± 0.19
[LDH2014] Fnx-mem0539	-0.74 ± 0.16	2.01 ± 0.21	WEL 60	-0.49 ± 0.09	1.98 ± 0.14
[LHT2010] BL138	-0.74 ± 0.03	1.81 ± 0.11	2MASS J02394309-3440186	-0.49 ± 0.08	1.92 ± 0.13
FBW J024006.1-342852	-0.74 ± 0.09	1.70 ± 0.13	2MASS J02393412-3433096	-0.48 ± 0.08	2.04 ± 0.12
[WMO2006] F01-6	-0.73 ± 0.07	1.91 ± 0.24	[LDH2014] Fnx-mem0522	-0.47 ± 0.06	1.96 ± 0.17
[LHT2010] BL104	-0.73 ± 0.09	1.81 ± 0.19	[LHT2010] BL298	-0.46 ± 0.06	1.93 ± 0.18
[WMO2009] For-0952	-0.73 ± 0.04	1.74 ± 0.20	2MASS J02395732-3431211	-0.43 ± 0.07	2.10 ± 0.22
2MASS J02382132-3436180	-0.73 ± 0.12	1.64 ± 0.19	[WMO2009] For-0949	-0.42 ± 0.08	1.99 ± 0.15
[LHT2010] BL146	-0.73 ± 0.08	1.77 ± 0.17	[WMO2006] F01-16	-0.38 ± 0.06	2.02 ± 0.18
[WMO2009] For-1208	-0.72 ± 0.06	1.90 ± 0.17	[LHT2010] BL163	-0.35 ± 0.07	1.86 ± 0.15
[WMO2009] For-1117	-0.72 ± 0.06	1.90 ± 0.19	2MASS J02393084-3435451	-0.35 ± 0.06	2.20 ± 0.20
GB07 Fnx24	-0.72 ± 0.08	1.51 ± 0.13	[MOW91] 21	-0.31 ± 0.11	2.00 ± 0.25
[LDH2014] Fnx-mem0754	-0.72 ± 0.05	1.80 ± 0.17			

- Arlandini, C., Käppeler, F., Wisshak, K., et al. 1999, *ApJ*, 525, 886, doi: [10.1086/307938](https://doi.org/10.1086/307938)
- Asplund, M., Grevesse, N., Sauval, A. J., & Scott, P. 2009, *ARA&A*, 47, 481, doi: [10.1146/annurev.astro.46.060407.145222](https://doi.org/10.1146/annurev.astro.46.060407.145222)
- Battaglia, G., Tolstoy, E., Helmi, A., et al. 2006, *A&A*, 459, 423, doi: [10.1051/0004-6361:20065720](https://doi.org/10.1051/0004-6361:20065720)
- Beers, T. C., & Christlieb, N. 2005, *ARA&A*, 43, 531, doi: [10.1146/annurev.astro.42.053102.134057](https://doi.org/10.1146/annurev.astro.42.053102.134057)
- Beniamini, P., Hotokezaka, K., & Piran, T. 2016, *ApJ*, 832, 149, doi: [10.3847/0004-637X/832/2/149](https://doi.org/10.3847/0004-637X/832/2/149)
- Beniamini, P., & Piran, T. 2019, *MNRAS*, 487, 4847, doi: [10.1093/mnras/stz1589](https://doi.org/10.1093/mnras/stz1589)
- Biemont, E., Grevesse, N., Hannaford, P., & Lowe, R. M. 1981, *ApJ*, 248, 867, doi: [10.1086/159213](https://doi.org/10.1086/159213)
- Bisterzo, S., Travaglio, C., Gallino, R., Wiescher, M., & Käppeler, F. 2014, *ApJ*, 787, 10, doi: [10.1088/0004-637X/787/1/10](https://doi.org/10.1088/0004-637X/787/1/10)
- Boeche, C., & Grebel, E. K. 2016, *A&A*, 587, A2, doi: [10.1051/0004-6361/201526758](https://doi.org/10.1051/0004-6361/201526758)
- Bouchard, A., Carignan, C., & Staveley-Smith, L. 2006, *AJ*, 131, 2913, doi: [10.1086/503629](https://doi.org/10.1086/503629)
- Bovard, L., Martin, D., Guercilena, F., et al. 2017, *PhRvD*, 96, 124005, doi: [10.1103/PhysRevD.96.124005](https://doi.org/10.1103/PhysRevD.96.124005)
- Cayrel, R., Depagne, E., Spite, M., et al. 2004, *A&A*, 416, 1117, doi: [10.1051/0004-6361:20034074](https://doi.org/10.1051/0004-6361:20034074)
- Coleman, M., Da Costa, G. S., Bland-Hawthorn, J., et al. 2004, *AJ*, 127, 832, doi: [10.1086/381298](https://doi.org/10.1086/381298)
- Coleman, M. G., & de Jong, J. T. A. 2008, *ApJ*, 685, 933, doi: [10.1086/589992](https://doi.org/10.1086/589992)
- Corliss, C. H., & Bozman, W. R. 1962, Experimental transition probabilities for spectral lines of seventy elements; derived from the NBS Tables of spectral-line intensities
- Côté, B., Fryer, C. L., Belczynski, K., et al. 2018, *ApJ*, 855, 99, doi: [10.3847/1538-4357/aaad67](https://doi.org/10.3847/1538-4357/aaad67)
- Côté, B., Eichler, M., Arcones, A., et al. 2019, *ApJ*, 875, 106, doi: [10.3847/1538-4357/ab10db](https://doi.org/10.3847/1538-4357/ab10db)
- Côté, B., Eichler, M., Yagüe López, A., et al. 2021, *Science*, 371, 945, doi: [10.1126/science.aba1111](https://doi.org/10.1126/science.aba1111)
- Cristallo, S., Abia, C., Straniero, O., & Piersanti, L. 2015, *ApJ*, 801, 53, doi: [10.1088/0004-637X/801/1/53](https://doi.org/10.1088/0004-637X/801/1/53)
- Cristallo, S., Piersanti, L., Straniero, O., et al. 2011, *ApJS*, 197, 17, doi: [10.1088/0067-0049/197/2/17](https://doi.org/10.1088/0067-0049/197/2/17)
- de Boer, T. J. L., Tolstoy, E., Hill, V., et al. 2012, *A&A*, 539, A103, doi: [10.1051/0004-6361/201118378](https://doi.org/10.1051/0004-6361/201118378)
- den Hartog, E. A., Curry, J. J., Wickcliffe, M. E., & Lawler, J. E. 1998, *SoPh*, 178, 239, doi: [10.1023/A:1005088315480](https://doi.org/10.1023/A:1005088315480)
- Den Hartog, E. A., Lawler, J. E., Sneden, C., & J., C. J. 2003, *The Astrophysical Journal Supplement Series*, 148, 543, doi: [10.1086/376940](https://doi.org/10.1086/376940)
- Denissenkov, P. A., Herwig, F., Battino, U., et al. 2017, *ApJL*, 834, L10, doi: [10.3847/2041-8213/834/2/L10](https://doi.org/10.3847/2041-8213/834/2/L10)
- Denissenkov, P. A., Herwig, F., Woodward, P., et al. 2019, *MNRAS*, 488, 4258, doi: [10.1093/mnras/stz1921](https://doi.org/10.1093/mnras/stz1921)
- Doherty, C. L., Gil-Pons, P., Siess, L., Lattanzio, J. C., & Lau, H. H. B. 2015, *MNRAS*, 446, 2599, doi: [10.1093/mnras/stu2180](https://doi.org/10.1093/mnras/stu2180)
- Duflo, J., & Zuker, A. P. 1995, *PhRvC*, 52, R23, doi: [10.1103/PhysRevC.52.R23](https://doi.org/10.1103/PhysRevC.52.R23)
- Edvardsson, B., Andersen, J., Gustafsson, B., et al. 1993, *A&AS*, 102, 603
- Eichler, M., & Arcones, A. 2021, Detailed abundances based on different nuclear physics for theoretical r-process scenarios, Zenodo, doi: [10.5281/zenodo.4446099](https://doi.org/10.5281/zenodo.4446099)
- Eichler, M., Sayar, W., Arcones, A., & Rauscher, T. 2019, *ApJ*, 879, 47, doi: [10.3847/1538-4357/ab24cf](https://doi.org/10.3847/1538-4357/ab24cf)
- Ezzeddine, R., Rasmussen, K., Frebel, A., et al. 2020, *ApJ*, 898, 150, doi: [10.3847/1538-4357/ab9d1a](https://doi.org/10.3847/1538-4357/ab9d1a)
- Fulbright, J. P. 2000, *AJ*, 120, 1841, doi: [10.1086/301548](https://doi.org/10.1086/301548)
- Gaia Collaboration. 2018a, *A&A*, 616, A1, doi: [10.1051/0004-6361/201833051](https://doi.org/10.1051/0004-6361/201833051)
- . 2018b, *VizieR Online Data Catalog*, I/345
- Geisler, D., Smith, V. V., Wallerstein, G., Gonzalez, G., & Charbonnel, C. 2005, *AJ*, 129, 1428, doi: [10.1086/427540](https://doi.org/10.1086/427540)
- Goriely, S., Bauswein, A., & Janka, H.-T. 2011, *ApJL*, 738, L32, doi: [10.1088/2041-8205/738/2/L32](https://doi.org/10.1088/2041-8205/738/2/L32)
- Gratton, R. G., & Sneden, C. 1988, *A&A*, 204, 193
- Grebel, E. K. 1997, *Reviews in Modern Astronomy*, 10, 29
- Hampel, M., Stancliffe, R. J., Lugaro, M., & Meyer, B. S. 2016, *ApJ*, 831, 171, doi: [10.3847/0004-637X/831/2/171](https://doi.org/10.3847/0004-637X/831/2/171)
- Hannaford, P., Lowe, R. M., Grevesse, N., Biemont, E., & Whaling, W. 1982, *ApJ*, 261, 736, doi: [10.1086/160384](https://doi.org/10.1086/160384)
- Hansen, C. J., El-Souri, M., Monaco, L., et al. 2018, *ApJ*, 855, 83, doi: [10.3847/1538-4357/aa978f](https://doi.org/10.3847/1538-4357/aa978f)
- Hansen, C. J., Primas, F., Hartman, H., et al. 2012, *A&A*, 545, A31, doi: [10.1051/0004-6361/201118643](https://doi.org/10.1051/0004-6361/201118643)
- Hansen, C. J., Koch, A., Mashonkina, L., et al. 2020, *A&A*, 643, A49, doi: [10.1051/0004-6361/202038805](https://doi.org/10.1051/0004-6361/202038805)
- Hendricks, B., Koch, A., Walker, M., et al. 2014, *A&A*, 572, A82, doi: [10.1051/0004-6361/201424645](https://doi.org/10.1051/0004-6361/201424645)
- Ishigaki, M. N., Aoki, W., & Chiba, M. 2013, *ApJ*, 771, 67, doi: [10.1088/0004-637X/771/1/67](https://doi.org/10.1088/0004-637X/771/1/67)
- Ivans, I. I., Sneden, C., James, C. R., et al. 2003, *ApJ*, 592, 906, doi: [10.1086/375812](https://doi.org/10.1086/375812)
- Ji, A. P., Frebel, A., Chiti, A., & Simon, J. D. 2016a, *Nature*, 531, 610, doi: [10.1038/nature17425](https://doi.org/10.1038/nature17425)

- Ji, A. P., Frebel, A., Simon, J. D., & Chiti, A. 2016b, *ApJ*, 830, 93, doi: [10.3847/0004-637X/830/2/93](https://doi.org/10.3847/0004-637X/830/2/93)
- Johnson, C. I., McWilliam, A., & Rich, R. M. 2013, *ApJL*, 775, L27, doi: [10.1088/2041-8205/775/1/L27](https://doi.org/10.1088/2041-8205/775/1/L27)
- Just, O., Goriely, S., Janka, H.-T., Nagataki, S., & Bauswein, A. 2021, arXiv e-prints, arXiv:2102.08387. <https://arxiv.org/abs/2102.08387>
- Karczmarek, P., Pietrzyński, G., Górski, M., Gieren, W., & Bersier, D. 2017, *AJ*, 154, 263, doi: [10.3847/1538-3881/aa9574](https://doi.org/10.3847/1538-3881/aa9574)
- Kathirgamaraju, A., Giannios, D., & Beniamini, P. 2019, *MNRAS*, 487, 3914, doi: [10.1093/mnras/stz1564](https://doi.org/10.1093/mnras/stz1564)
- Kellicott, A., Ricciardi, M. V., & Schmidt, K. H. 2008, in *Dynamical Aspects of Nuclear Fission*, 203–215, doi: [10.1142/9789812837530_0016](https://doi.org/10.1142/9789812837530_0016)
- Kirby, E. N., Guhathakurta, P., Simon, J. D., et al. 2010, *ApJS*, 191, 352, doi: [10.1088/0067-0049/191/2/352](https://doi.org/10.1088/0067-0049/191/2/352)
- Kobayashi, C., Karakas, A. I., & Lugaro, M. 2020, *ApJ*, 900, 179, doi: [10.3847/1538-4357/abae65](https://doi.org/10.3847/1538-4357/abae65)
- Kobayashi, C., Umeda, H., Nomoto, K., Tominaga, N., & Ohkubo, T. 2006, *ApJ*, 653, 1145, doi: [10.1086/508914](https://doi.org/10.1086/508914)
- Koch, A., Reichert, M., Hansen, C. J., et al. 2019, *A&A*, 622, A159, doi: [10.1051/0004-6361/201834241](https://doi.org/10.1051/0004-6361/201834241)
- Kodama, T., & Takahashi, K. 1975, *NuPhA*, 239, 489, doi: [10.1016/0375-9474\(75\)90381-4](https://doi.org/10.1016/0375-9474(75)90381-4)
- Korobkin, O., Rosswog, S., Arcones, A., & Winteler, C. 2012, *MNRAS*, 426, 1940, doi: [10.1111/j.1365-2966.2012.21859.x](https://doi.org/10.1111/j.1365-2966.2012.21859.x)
- Kurucz, R. L. 1970, *SAO Special Report*, 309
- . 2011, *Canadian Journal of Physics*, 89, 417, doi: [10.1139/p10-104](https://doi.org/10.1139/p10-104)
- Lawler, J. E., Bonvallet, G., & Sneden, C. 2001, *ApJ*, 556, 452, doi: [10.1086/321549](https://doi.org/10.1086/321549)
- Lawler, J. E., & Dakin, J. T. 1989, *J. Opt. Soc. Am. B*, 6, 1457, doi: [10.1364/JOSAB.6.001457](https://doi.org/10.1364/JOSAB.6.001457)
- Lawler, J. E., Sneden, C., & Cowan, J. J. 2015, *ApJS*, 220, 13, doi: [10.1088/0067-0049/220/1/13](https://doi.org/10.1088/0067-0049/220/1/13)
- Lawler, J. E., Sneden, C., Cowan, J. J., Ivans, I. I., & Den Hartog, E. A. 2009, *ApJS*, 182, 51, doi: [10.1088/0067-0049/182/1/51](https://doi.org/10.1088/0067-0049/182/1/51)
- Lemasle, B., de Boer, T. J. L., Hill, V., et al. 2014, *A&A*, 572, A88, doi: [10.1051/0004-6361/201423919](https://doi.org/10.1051/0004-6361/201423919)
- Letarte, B., Hill, V., Tolstoy, E., et al. 2010, *A&A*, 523, A17, doi: [10.1051/0004-6361/200913413](https://doi.org/10.1051/0004-6361/200913413)
- . 2018, *A&A*, 613, C1, doi: [10.1051/0004-6361/200913413e](https://doi.org/10.1051/0004-6361/200913413e)
- Lokas, E. L. 2009, *MNRAS*, 394, L102, doi: [10.1111/j.1745-3933.2009.00620.x](https://doi.org/10.1111/j.1745-3933.2009.00620.x)
- Mackey, A. D., & Gilmore, G. F. 2003, *MNRAS*, 340, 175, doi: [10.1046/j.1365-8711.2003.06275.x](https://doi.org/10.1046/j.1365-8711.2003.06275.x)
- Magg, M., Nordlander, T., Glover, S. C. O., et al. 2020, *MNRAS*, 498, 3703, doi: [10.1093/mnras/staa2624](https://doi.org/10.1093/mnras/staa2624)
- Marketin, T., Huther, L., & Martínez-Pinedo, G. 2016, *PhRvC*, 93, 025805, doi: [10.1103/PhysRevC.93.025805](https://doi.org/10.1103/PhysRevC.93.025805)
- Matteucci, F., Romano, D., Arcones, A., Korobkin, O., & Rosswog, S. 2014, *MNRAS*, 438, 2177, doi: [10.1093/mnras/stt2350](https://doi.org/10.1093/mnras/stt2350)
- McConnachie, A. W., & Venn, K. A. 2020, *AJ*, 160, 124, doi: [10.3847/1538-3881/aba4ab](https://doi.org/10.3847/1538-3881/aba4ab)
- McWilliam, A., Preston, G. W., Sneden, C., & Shectman, S. 1995, *AJ*, 109, 2736, doi: [10.1086/117485](https://doi.org/10.1086/117485)
- Meggers, W. F., Corliss, C. H., & Scribner, B. F. 1975, *Tables of spectral-line intensities. Part I, II- arranged by elements.*
- Miller, J. M., Sprouse, T. M., Fryer, C. L., et al. 2020, *ApJ*, 902, 66, doi: [10.3847/1538-4357/abb4e3](https://doi.org/10.3847/1538-4357/abb4e3)
- Möller, P., Pfeiffer, B., & Kratz, K.-L. 2003, *PhRvC*, 67, 055802, doi: [10.1103/PhysRevC.67.055802](https://doi.org/10.1103/PhysRevC.67.055802)
- Mösta, P., Roberts, L. F., Halevi, G., et al. 2018, *ApJ*, 864, 171, doi: [10.3847/1538-4357/aad6ec](https://doi.org/10.3847/1538-4357/aad6ec)
- NED Team. 2007, in *Astronomical Society of the Pacific Conference Series*, Vol. 376, *Astronomical Data Analysis Software and Systems XVI*, ed. R. A. Shaw, F. Hill, & D. J. Bell, 153
- Nishimura, N., Sawai, H., Takiwaki, T., Yamada, S., & Thielemann, F. K. 2017, *ApJ*, 836, L21, doi: [10.3847/2041-8213/aa5dee](https://doi.org/10.3847/2041-8213/aa5dee)
- Nishimura, N., Takiwaki, T., & Thielemann, F.-K. 2015, *ApJ*, 810, 109, doi: [10.1088/0004-637X/810/2/109](https://doi.org/10.1088/0004-637X/810/2/109)
- Nissen, P. E., Hoeg, E., & Schuster, W. J. 1997, in *ESA Special Publication*, Vol. 402, *Hipparcos - Venice '97*, ed. R. M. Bonnet, E. Høg, P. L. Bernacca, L. Emiliani, A. Blaauw, C. Turon, J. Kovalevsky, L. Lindgren, H. Hassan, M. Bouffard, B. Strim, D. Heger, M. A. C. Perryman, & L. Woltjer, 225–230
- Nomoto, K., Tominaga, N., Umeda, H., Kobayashi, C., & Maeda, K. 2006, *NuPhA*, 777, 424, doi: [10.1016/j.nuclphysa.2006.05.008](https://doi.org/10.1016/j.nuclphysa.2006.05.008)
- Panov, I. V., Freiburghaus, C., & Thielemann, F. K. 2001, *NuPhA*, 688, 587, doi: [10.1016/S0375-9474\(01\)00797-7](https://doi.org/10.1016/S0375-9474(01)00797-7)
- Pasquini, L., Avila, G., Blecha, A., et al. 2002, *The Messenger*, 110, 1
- Prochaska, J. X., Naumov, S. O., Carney, B. W., McWilliam, A., & Wolfe, A. M. 2000, *AJ*, 120, 2513, doi: [10.1086/316818](https://doi.org/10.1086/316818)
- Reddy, B. E., Lambert, D. L., & Allende Prieto, C. 2006, *MNRAS*, 367, 1329, doi: [10.1111/j.1365-2966.2006.10148.x](https://doi.org/10.1111/j.1365-2966.2006.10148.x)

- Reddy, B. E., Tomkin, J., Lambert, D. L., & Allende Prieto, C. 2003, *MNRAS*, 340, 304, doi: [10.1046/j.1365-8711.2003.06305.x](https://doi.org/10.1046/j.1365-8711.2003.06305.x)
- Reichert, M., Hansen, C. J., Hanke, M., et al. 2020, *A&A*, 641, A127, doi: [10.1051/0004-6361/201936930](https://doi.org/10.1051/0004-6361/201936930)
- Reichert, M., Obergaulinger, M., Eichler, M., Aloy, M. Á., & Arcones, A. 2021, *MNRAS*, 501, 5733, doi: [10.1093/mnras/stab029](https://doi.org/10.1093/mnras/stab029)
- Roederer, I. U., Hattori, K., & Valluri, M. 2018a, *AJ*, 156, 179, doi: [10.3847/1538-3881/aadd9c](https://doi.org/10.3847/1538-3881/aadd9c)
- Roederer, I. U., Sakari, C. M., Placco, V. M., et al. 2018b, *ApJ*, 865, 129, doi: [10.3847/1538-4357/aadd92](https://doi.org/10.3847/1538-4357/aadd92)
- Roederer, I. U., Mateo, M., Bailey, John I., I., et al. 2016, *AJ*, 151, 82, doi: [10.3847/0004-6256/151/3/82](https://doi.org/10.3847/0004-6256/151/3/82)
- Rusakov, V., Monelli, M., Gallart, C., et al. 2021, *MNRAS*, 502, 642, doi: [10.1093/mnras/stab006](https://doi.org/10.1093/mnras/stab006)
- Ryan, S. G., Norris, J. E., & Beers, T. C. 1996, *ApJ*, 471, 254, doi: [10.1086/177967](https://doi.org/10.1086/177967)
- Sadakane, K., Arimoto, N., Ikuta, C., et al. 2004, *PASJ*, 56, 1041, doi: [10.1093/pasj/56.6.1041](https://doi.org/10.1093/pasj/56.6.1041)
- Shetrone, M. D., Côté, P., & Sargent, W. L. W. 2001, *ApJ*, 548, 592, doi: [10.1086/319022](https://doi.org/10.1086/319022)
- Shibata, M., & Hotokezaka, K. 2019, *Annual Review of Nuclear and Particle Science*, 69, 41, doi: [10.1146/annurev-nucl-101918-023625](https://doi.org/10.1146/annurev-nucl-101918-023625)
- Siegel, D. M., Barnes, J., & Metzger, B. D. 2019, *Nature*, 569, 241, doi: [10.1038/s41586-019-1136-0](https://doi.org/10.1038/s41586-019-1136-0)
- Skúladóttir, Á., Hansen, C. J., Choplin, A., et al. 2020, *A&A*, 634, A84, doi: [10.1051/0004-6361/201937075](https://doi.org/10.1051/0004-6361/201937075)
- Snedden, C. 1973, *ApJ*, 184, 839, doi: [10.1086/152374](https://doi.org/10.1086/152374)
- Snedden, C., Cowan, J. J., & Gallino, R. 2008, *ARA&A*, 46, 241, doi: [10.1146/annurev.astro.46.060407.145207](https://doi.org/10.1146/annurev.astro.46.060407.145207)
- Stancliffe, R. J., Dearborn, D. S. P., Lattanzio, J. C., Heap, S. A., & Campbell, S. W. 2011, *ApJ*, 742, 121, doi: [10.1088/0004-637X/742/2/121](https://doi.org/10.1088/0004-637X/742/2/121)
- Stephens, A., & Boesgaard, A. M. 2002, *AJ*, 123, 1647, doi: [10.1086/338898](https://doi.org/10.1086/338898)
- Suda, T., Hidaka, J., Aoki, W., et al. 2017, *PASJ*, 69, 76, doi: [10.1093/pasj/psx059](https://doi.org/10.1093/pasj/psx059)
- Tolstoy, E., Hill, V., & Tosi, M. 2009, *ARA&A*, 47, 371, doi: [10.1146/annurev-astro-082708-101650](https://doi.org/10.1146/annurev-astro-082708-101650)
- Tsujimoto, T., & Shigeyama, T. 2002, *ApJL*, 571, L93, doi: [10.1086/341370](https://doi.org/10.1086/341370)
- van de Voort, F., Pakmor, R., Grand, R. J. J., et al. 2020, *MNRAS*, 494, 4867, doi: [10.1093/mnras/staa754](https://doi.org/10.1093/mnras/staa754)
- Velichko, A. B., Mashonkina, L. I., & Nilsson, H. 2010, *Astronomy Letters*, 36, 664, doi: [10.1134/S1063773710090057](https://doi.org/10.1134/S1063773710090057)
- Watson, D., Hansen, C. J., Selsing, J., et al. 2019, *Nature*, 574, 497, doi: [10.1038/s41586-019-1676-3](https://doi.org/10.1038/s41586-019-1676-3)
- Weisz, D. R., Dolphin, A. E., Skillman, E. D., et al. 2014, *ApJ*, 789, 147, doi: [10.1088/0004-637X/789/2/147](https://doi.org/10.1088/0004-637X/789/2/147)
- Wenger, M., Ochsenbein, F., Egret, D., et al. 2000, *Astronomy and Astrophysics Supplement Series*, 143, 9, doi: [10.1051/aas:2000332](https://doi.org/10.1051/aas:2000332)
- Winteler, C., Käppeli, R., Peregó, A., et al. 2012, *ApJL*, 750, L22, doi: [10.1088/2041-8205/750/1/L22](https://doi.org/10.1088/2041-8205/750/1/L22)
- Wu, M.-R., Fernández, R., Martínez-Pinedo, G., & Metzger, B. D. 2016, *MNRAS*, 463, 2323, doi: [10.1093/mnras/stw2156](https://doi.org/10.1093/mnras/stw2156)
- Xing, Q.-F., Zhao, G., Aoki, W., et al. 2019, *Nature Astronomy*, 3, 631, doi: [10.1038/s41550-019-0764-5](https://doi.org/10.1038/s41550-019-0764-5)